Branched Pectic Galactan in Phloem-Sieve-Element Cell Walls: Implications for Cell Mechanics[1][CC-BY]

Thomas A. Torode,[a,b,2] Rachel O'Neill,[a,c,2] Susan E. Marcus,[a] Valérie Cornuault,[a] Sara Pose,[a]
Rebecca P. Lauder,[c] Stjepan K. Kračun,[d] Maja Gro Rydahl,[d] Mathias C. F. Andersen,[e] William G. T. Willats,[f]
Siobhan A. Braybrook,[b] Belinda J. Townsend,[c] Mads H. Clausen,[e] and J. Paul Knox[a]

[a]Centre for Plant Sciences, Faculty of Biological Sciences, University of Leeds, Leeds LS2 9JT, United Kingdom
[b]Sainsbury Laboratory, University of Cambridge, Cambridge, CB2 1LR, United Kingdom
[c]Department of Plant Biology and Crop Science, Rothamsted Research, Harpenden, Hertfordshire, AL5 2JQ, United Kingdom
[d]Department of Plant and Environmental Sciences, University of Copenhagen, Frederiksberg 1871, Denmark
[e]Center for Nanomedicine and Theranostics, Department of Chemistry, Technical University of Denmark, Kemitorvet, DK-2800 Kgs. Lyngby, Denmark
[f]School of Agriculture, Food and Rural Development, Newcastle University, Newcastle upon Tyne NE1 7RU, UK

ORCID IDs: 0000-0002-8295-3088 (S.P.); 0000-0002-5795-1320 (S.K.K.); 0000-0002-4308-5580 (S.A.B.); 0000-0001-9649-1729 (M.H.C.); 0000-0002-9231-6891 (J.P.K.).

A major question in plant biology concerns the specification and functional differentiation of cell types. This is in the context of constraints imposed by networks of cell walls that both adhere cells and contribute to the form and function of developing organs. Here, we report the identification of a glycan epitope that is specific to phloem sieve element cell walls in several systems. A monoclonal antibody, designated LM26, binds to the cell wall of phloem sieve elements in stems of Arabidopsis (*Arabidopsis thaliana*), *Miscanthus* x *giganteus*, and notably sugar beet (*Beta vulgaris*) roots where phloem identification is an important factor for the study of phloem unloading of Suc. Using microarrays of synthetic oligosaccharides, the LM26 epitope has been identified as a β-1,6-galactosyl substitution of β-1,4-galactan requiring more than three backbone residues for optimized recognition. This branched galactan structure has previously been identified in garlic (*Allium sativum*) bulbs in which the LM26 epitope is widespread throughout most cell walls including those of phloem cells. Garlic bulb cell wall material has been used to confirm the association of the LM26 epitope with cell wall pectic rhamnogalacturonan-I polysaccharides. In the phloem tissues of grass stems, the LM26 epitope has a complementary pattern to that of the LM5 linear β-1,4-galactan epitope, which is detected only in companion cell walls. Mechanical probing of transverse sections of *M.* x *giganteus* stems and leaves by atomic force microscopy indicates that phloem sieve element cell walls have a lower indentation modulus (indicative of higher elasticity) than companion cell walls.

The mechanistic basis of primary cell wall heterogeneity in the context of cell type differentiation and cell function is a poorly understood factor in plant development. Plant cell walls are cellulosic composites that underpin and control many aspects of plant cell and organ growth by virtue of the presence of adherent cell surfaces that ramify throughout developing and mature organs. In addition to cellulosic fibers that provide structural strength to cell walls, several sets of noncellulosic matrix polysaccharides are present (Burton et al., 2010; Doblin et al., 2010). These are often structurally hypervariable and are important factors in cell wall biogenesis, cell extension, and cell function. Not all cell surfaces are the same in terms of precise structures of individual polysaccharides, and cell-wall glycan molecular configurations display developmental dynamics and cell type specificities (Burton et al., 2010; Knox 2008; Lee et al., 2012; Torode et al., 2016).

Cell wall matrix polysaccharides have been a focus for understanding cell wall heterogeneity and cell wall dynamics in relation to both growth and anatomical cell differentiation. Pectic polysaccharides are a major group of matrix polysaccharides, defined as galacturonic-acid-rich polymers, which comprise at least three major domains (Caffall and Mohnen 2009; Atmodjo et al., 2013). Homogalacturonan (HG) can be variably methyl-esterified and acetylated, and these modifications influence its interactions and supramolecular properties (Wolf et al., 2009). Rhamnogalacturonan-II is a largely taxonomically conserved, structurally highly complex region of HG with short side chain substitutions that can dimerize and link HG chains through borate esters (Caffall and Mohnen 2009). Rhamnogalacturonan-I (RG-I) is a hypervariable pectic polysaccharide with a rhamnosyl and galacturonosyl backbone with substitution by a complex array of side chains in which 1,4-galactosyl and or 1,5-arabinosyl residues often predominate (Yapo 2011; Lee et al., 2013). RG-I polysaccharides are widely distributed and studies in relation to cell functions have focused on

roles in generation of cell wall mechanical properties such as cell wall firmness and cell wall elasticity (McCartney et al., 2000; Lee et al., 2012). Noncellulosic and nonpectic polysaccharides, often grouped as hemicelluloses, include xyloglucans, heteroxylans, heteromannan, and mixed-linkage glucans and these also display structural variations and in some cases cell and tissue specificities in occurrence (Burton et al., 2010; Scheller and Ulvskov 2010).

Monoclonal antibodies (MAbs) are the most effective molecular tools to-date to explore and understand cell wall heterogeneity in cell and tissue contexts (Knox 2008; Pattathil et al., 2015; Torode et al., 2016). Pectic HG and pectic RG-I epitopes are widely distributed and have been related to cell dynamics influencing cell growth and cell adhesion (Knox 2008; Willats et al., 2001a) but are rarely specific to cell types across a wide range of species. Similarly, glycan moieties of arabinogalactan-protein (AGP) proteoglycans are known to be hypervariable, and AGP glycan epitopes have been documented to be intimately related to early developmental patterns including vascular differentiation (Knox et al., 1989; Showalter 2001), but precise association with cell types often varies between species and taxonomic groups (Casero et al., 1998; Knox 2006). Heteroxylan MAbs bind specifically to developing and mature xylem vessel elements and sclerenchyma fiber cells in eudicot systems by virtue of the presence of heteroxylan-rich secondary cell walls (McCartney et al., 2005). No cell wall markers are known for phloem sieve elements that maintain only a primary cell wall with no extensive cell wall elaborations other than the elaboration of sieve plates, and in some cases a thickening of primary cell walls relative to adjacent cells (Evert 2006; Mullendore et al., 2010; Truernit 2014). Hence, the identification of phloem cells can be particularly challenging.

Here we report the isolation of a MAb, LM26, which binds specifically to phloem sieve elements in several important systems including sugar beet storage roots, grass stems including the bioenergy crop *Miscanthus x giganteus* (hereafter Miscanthus), and Arabidopsis (*Arabidopsis thaliana*) inflorescence stems. Use of microarrays populated with synthetic oligosaccharides has facilitated the identification of the glycan structure bound by LM26 as a β-1,6-galactosyl substitution of 1,4-galactan. A wider abundance of the LM26 epitope in garlic (*Allium sativum*) bulb cell walls has enabled chromatographic analyses of isolated polymers and confirmation of the association of the LM26 epitope with 1,4-galactan and RG-I glycans. Mechanical testing of the phloem tissue of Miscanthus in which phloem sieve elements are interspersed with companion cells is indicative of an increased relative elasticity of the phloem sieve element cell walls.

RESULTS

Monoclonal Antibody LM26 Binds Specifically to Phloem Sieve Elements in a Range of Plant Organs Including Sugar Beet Roots

A wide-scale screen of MAbs secreted by cell lines derived subsequent to immunizations with a range of plant cell wall-derived/related immunogens was undertaken to isolate antibodies with novel specificities. A cell line, arising from the immunization that led to the isolation of the pectic homogalacturonan MAb LM7 (Willats et al., 2001b), was found to secrete a MAb with the capacity to bind to plant cell walls. In the case of transverse sections of Arabidopsis (eudicot, rosid, Brassicaceae) inflorescence stems, its binding was specific to phloem sieve elements (Fig. 1). This antibody was designated LM26 and its specificity toward phloem sieve elements was found to occur in a wide range of plant species and organs encompassing tomato (eudicot, asterid, Solanaceae) petiole and grass stems including Miscanthus (commelinid monocotyledon, Poaceae) as shown in Figure 1. In the case of transverse sections of grass stems, the LM26 epitope is detected at the surface of sieve elements in the phloem bundles and not the associated companion cells. During the characterization of LM26 binding to phloem sieve elements of grass stems, it was noted that the companion cells were specifically labeled by a MAb to pectic 1,4-galactan (LM5) generating an immunolabeling pattern
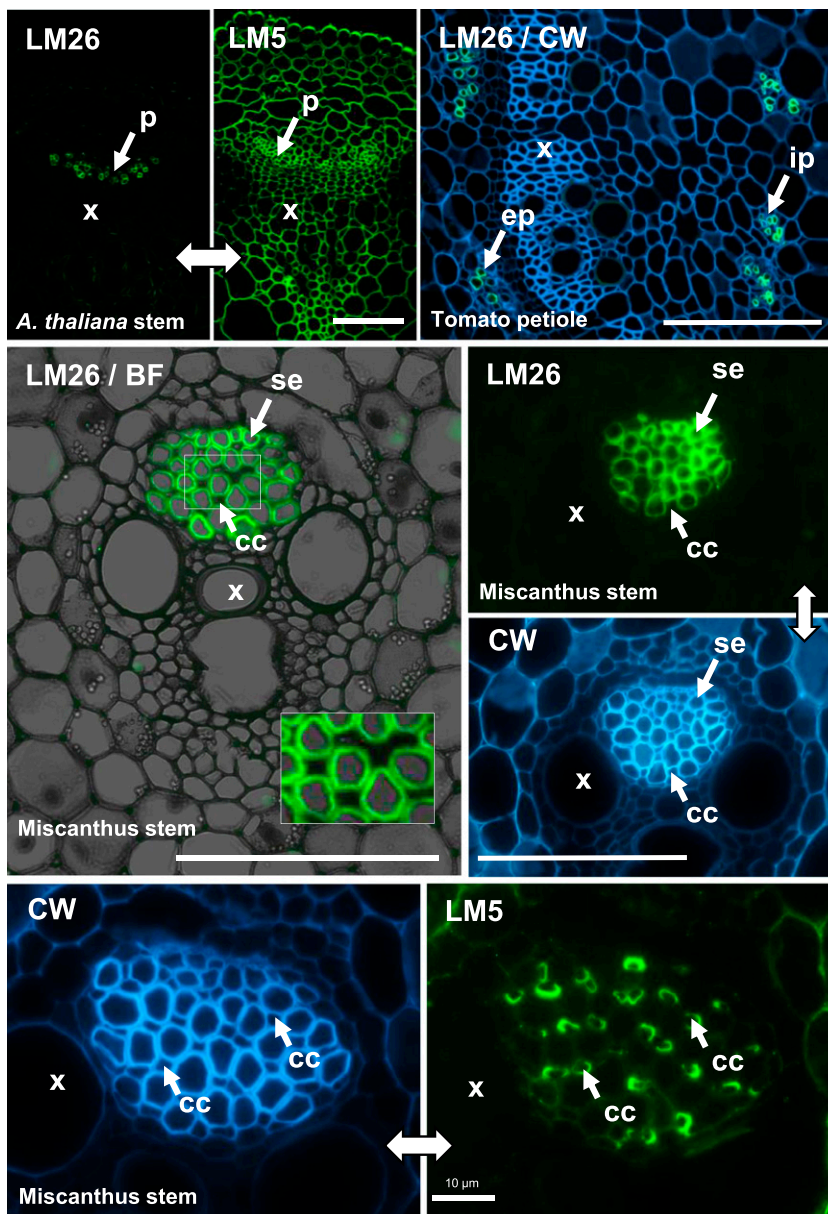
Figure 1. Indirect immunofluorescence analysis of MAb LM26 binding to transverse sections of Arabidopsis inflorescence stem, tomato leaf petiole, and *M.* x *giganteus* stem. In these organs the LM26 epitope is specific to phloem sieve elements. In the case of Arabidopsis and *M.* x. *giganteus*, stem immunolabeling by LM5 is shown for comparative purposes. Blue fluorescence is from Calcofluor White staining of all cells. Double magnification image inset in *M.* x *giganteus* LM26/bright-field panel to show absence of LM26 epitope in companion cells. Bars = 100 μm unless indicated otherwise. Double-ended arrows linking micrographs indicate same or equivalent sections. BF, bright field; cc, phloem companion cells; CW, Calcofluor White; ep, external phloem; ip, internal phloem; p, phloem; se, sieve element, x, xylem vessel element.

complementary to that of LM26 (Fig. 1). This complementary labeling pattern with LM26 and LM5 has not been observed to-date in species other than grasses. Equivalent specific recognition of sieve elements by LM26 and companion cells by LM5 in phloem regions of maize (*Zea mays*) stem is shown in Supplemental Data File S2. A notable feature of grass phloem tissue is the presence of only sieve elements and companion cells with no interspersed parenchyma cells that are abundant in eudicot phloem tissues.

The LM26 epitope was also found to be specific to phloem sieve elements of sugar beet storage roots as seen in transverse sections shown in Figure 2. Phloem abundance and Suc unloading are crucial elements

influencing the Suc yield of sugar beet (*Beta vulgaris* subsp. *vulgaris*: eudicot, Caryophyllales, Amaranthaceae) explained by the Suc-gradient hypothesis (Wyse 1979; Bell et al., 1996), and therefore in this system the identification and study of phloem cells has industrial importance. Sugar beet storage root growth involves the development of successive vascular cambia resulting in concentric rings of alternating phloem and xylem (Fig. 2). The analysis of sections of resin-embedded material confirmed the specific recognition of phloem sieve elements and not the adjacent companion cells with dense cytoplasm (Fig. 2). Immunogold labeling of the LM26 epitope in phloem sieve elements indicated its
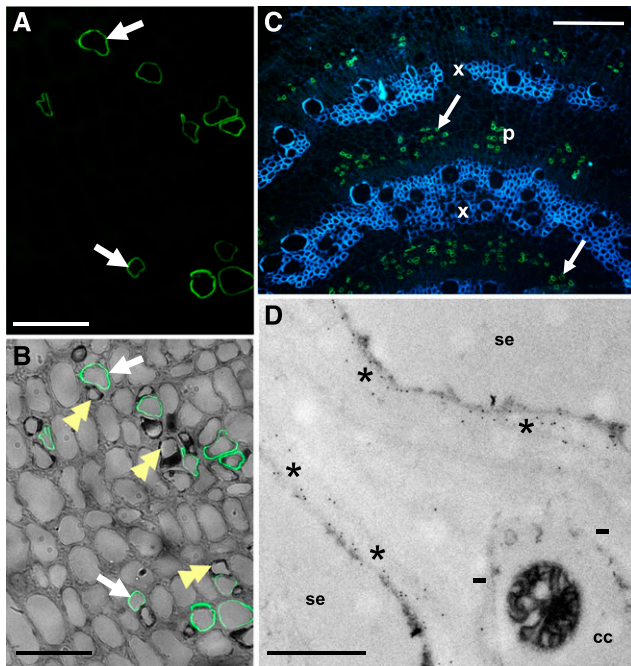
Figure 2. Indirect in situ analyses of MAb LM26 binding to transverse sections of sugar beet storage root. A, Immunofluorescence (green FITC) of LM26 binding to isolated cells in a resin-embedded section. B, Same section as (A) with combined bright field/fluorescence. Arrows indicate phloem sieve elements bound by LM26 and pale yellow double arrowheads indicate associated companion cells with high cytoplasmic content. Bars = 20 μm. C, Combined image of LM26 fluorescence binding to phloem cells with bands of xylem cells stained blue with Calcofluor White. Successive cambia of sugar beet storage roots produce alternating xylem and phloem tissues. Bar = 400 μm. D, Transmission electron microscopy and immunogold labeling of LM26 binding to an intercambial region. Gold particles are restricted to the inner cell wall regions (marked with asterisks) of phloem sieve elements. The LM26 epitope is not present in the middle lamella or cell walls of neighboring companion cells as marked by dashes. Bar = 1.0 μm. cc, companion cells; p, phloem; se, sieve elements; x, xylem.

restriction to the inner third of cell walls adjacent to the plasma membrane (Fig. 2).

In summary, the LM26 rat MAb binds specifically to the cell wall of phloem sieve elements in a range of organs across widely diverged taxonomic groups of vascular plants.

LM26 Binds to a β-1,6-Galactosyl Substitution of Pectic β-1,4-Galactan, a Glycan Motif of Pectic Rhamnogalacturonan-I

To determine the structure recognized by LM26, the antibody was used to probe extensive sets of glycan microarrays with assembled sets of synthetic oligosaccharides relating to those found in plant cell wall glycans (Andersen et al., 2016a). The LM26 MAb was found to bind to three structurally related branched versions of oligo-β-1,4-galactosides. The most effective recognition was of 6'''-O-(β-Gal)-β-1,4-galactohexaose (oligo-12;

Fig. 3) with much weaker recognition in the case of more extended substitution (oligo-10; Fig. 3) or a shorter backbone (oligo-5; Fig. 3). The binding of the 1,4-galactan-specific MAb LM5 is shown for comparison and its recognition capabilities are restricted to the set of linear oligo-β-1,4-galactosides and not those with substitutions (Fig. 3), as recently reported (Andersen et al., 2016b), indicating the complementary recognition of branched and linear galactan chains by LM26 and LM5, respectively.

β-1,4-galactan is a structural element found in the side chains of RG-I that in turn is a substructure of the complex multidomain pectic polysaccharides that have abundant HG domains (Atmodjo et al., 2013). A β-1,6-galactosyl substitution of β-1,4-galactan structures is rare in pectic side chains of RG-I (Arifkhodzhaev 2000; Ridley et al., 2001) but has been identified in extracts of garlic bulbs (Das and Das, 1977). Analysis of sections of garlic bulb indicated that the LM26 epitope occurred in most cell walls (Supplemental Data File S1). As the LM26 epitope could not be extracted in a sufficient relative abundance for analyses from sugar beet roots, the abundant source of the LM26 epitope in garlic bulbs enabled additional analyses to confirm the association of the LM26 epitope with pectic glycans. The LM26 and the LM5 epitopes were found to be abundant in all fractions of an alcohol-insoluble residue (AIR) of garlic bulbs solubilized by extractants of increasing stringency. This indicates that the branched and linear galactan motifs are linked into the cell wall architecture by a range of mechanisms. Particular abundance of both galactan epitopes (LM5 and LM26) was observed in a LiCl/N,N-dimethylacetamide extraction of AIR (Fig. 4)—a postalkali extraction step aimed at extraction of polymers most tightly associated with cellulose microfibrils (Gurjanov et al., 2008). The first, water-soluble, isolate of the AIR had the highest relative enrichment of the LM26 epitope and this was used to explore the biochemical context of the epitope. LM26 was used as a detection tool (alongside other pectic oligosaccharide-directed probes including LM5) for polymers separated using microscale anion-exchange chromatography (a technique termed "epitope detection chromatography" (EDC; Cornuault et al., 2014). Fractions were eluted from the anion-exchange column with a stepped gradient of salt elution producing coinciding peaks for LM26, LM5, and the JIM7 epitope (Fig. 4). The MAb JIM7 binds to methyl-esterified HG (Clausen et al., 2003). The MAb LM19 binds to unesterified HG and its epitope elutes only at the highest salt concentration, indicating a distinct subset of unesterified HG (Fig. 4). A prechromatography alkali treatment to remove methyl esters from HG led to loss of the JIM7 epitope and an increase in signals coincident with the unesterified HG peak. In all cases the LM26 detection traces were highly similar to those of LM5, and both showed a shift to later elution after the deesterification treatment. In this analysis some LM26/LM5 epitopes did not coelute with the LM19 HG epitope after deesterification (Fig. 4),

Compound	1	2	3	4	5	6	7	8	9	10	11	12
Type	linear oligos				branched oligos							
LM26	0	0	0	0	21	0	0	0	0	18	0	100
LM5	100	81	51	0	0	0	0	0	0	0	0	0

1   β-1,4 galactotriose
2   β-1,4 galactopentaose
3   β-1,4 galactoheptaose
4   α-1,4 Araf-β-1,4 galactohexaose
5   6'-O-(β-1,6 Gal)-β-1,4 galactotriose
6   6'-O-(α-1,6 Gal)-β-1,4 galactotriose
7   4'-O-(α-1,4 Gal)-6'-O-(α-1,6 Gal)-β-1,4 galactobiose
8   6'''-O-(α-1,6 Araf)-β-1,4 galactohexaose
9   6'''-O-(α-1,5 Araf-α-1,6 Araf)-β-1,4 galactohexaose
10 6'''-O-(β-1,6 Gal-β-1,6 Gal)-β-1,4 galactohexaose
11 6'''-O-(β-1,4 Gal-β-1,6 Gal)-β-1,4 galactohexaose
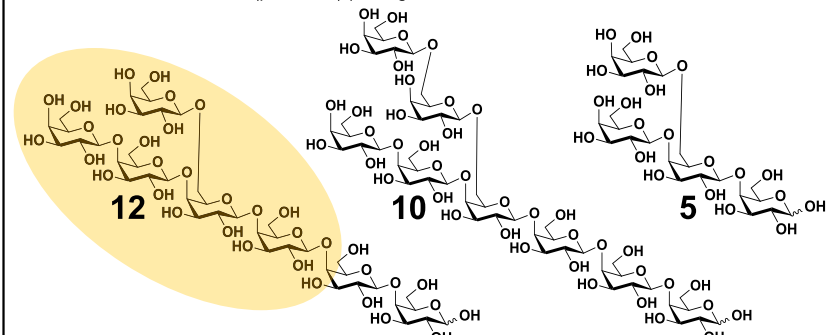12 6'''-O-(β-1,6 Gal)-β-1,4 galactohexaose

Figure 3. Glycan microarray analysis of the binding of MAbs LM5 and LM26 to 12 synthetic 1,4-galacto-oligosaccharides. Values shown are the % of the maximal detectable signal. Structures of the three branched oligosaccharides bound by LM26 are shown and the proposed LM26 epitope is marked by the shaded ellipse over oligosaccharide-12. LM5 binds to linear 1,4-galacto-oligosaccharides (Andersen et al., 2016b).

suggesting that not all RG-I domains are attached to abundant HG domains.

In summary, the LM26 MAb binds to a β-galactosyl substitution of 1,4-galactan associated with pectic RG-I. In the case of garlic bulb cell walls, the LM5 and LM26 epitopes are both widely distributed in cell wall fractions with a significant proportion tightly associated with cellulose microfibrils.

Nanomechanical Testing of Phloem Tissues in Miscanthus in Relation to the Complementary Patterning of LM5 Linear and LM26 Branched Galactan Epitopes

Complementary patterning of the LM5 linear galactan and LM26 branched galactan epitopes between companion cell walls and sieve element cell walls, respectively, is a feature of Miscanthus stem phloem tissues (Fig. 1). Immunogold analyses indicated that detection of the LM26 and LM5 epitopes was restricted to inner cell wall regions in this tissue, and in the case of the LM26 epitope it appeared to be restricted to a region very close to the plasma membrane (Fig. 5). To further explore the functional role of branched and linear galactan side chains of RG-I within cell walls, transverse sections of Miscanthus stems were subjected to mechanical testing using atomic force microscopy (AFM). As vascular tissues are internal plant organs, this required nanoindentation experiments to be performed on sectioned material. This approach has been successfully applied to sections of brain and insect wing (Christ et al., 2010; Sun et al., 2006).

Mapping of the elastic indentation modulus (IM; Cosgrove 2016) across vascular bundles (100 μm^2, 256^2 indentations; 390 nm resolution) revealed that the cell walls of the phloem are more elastic than both the surrounding sclerenchyma cells and xylem vessels (Fig. 6; lower IM equates to more elastic behavior). To distinguish between sieve elements and companion cells within the phloem tissue, higher resolution scans of phloem regions were performed (50 μm^2, 256^2 indentations; 195 nm resolution). Nanomechanical mapping at this resolution indicated that the sieve element cell walls had lower IM (were more elastic) than neighboring companion cell walls. Utilizing even higher resolution maps (10 μm^2, 256^2 indentations; 39 nm resolution), it was observed that sieve element cell walls displayed a spatial patterning of IM across the cell wall, with inner cell wall regions closest to the plasma membrane being the most elastic (Fig. 6). A transect across two adjacent sieve element cell walls indicated a clear reduction in IM toward the inner cell wall region, and particularly in the region closest to the plasma membrane (Fig. 6I).

As these studies were on fixed, wax-embedded stem materials, it was important to look at the equivalent
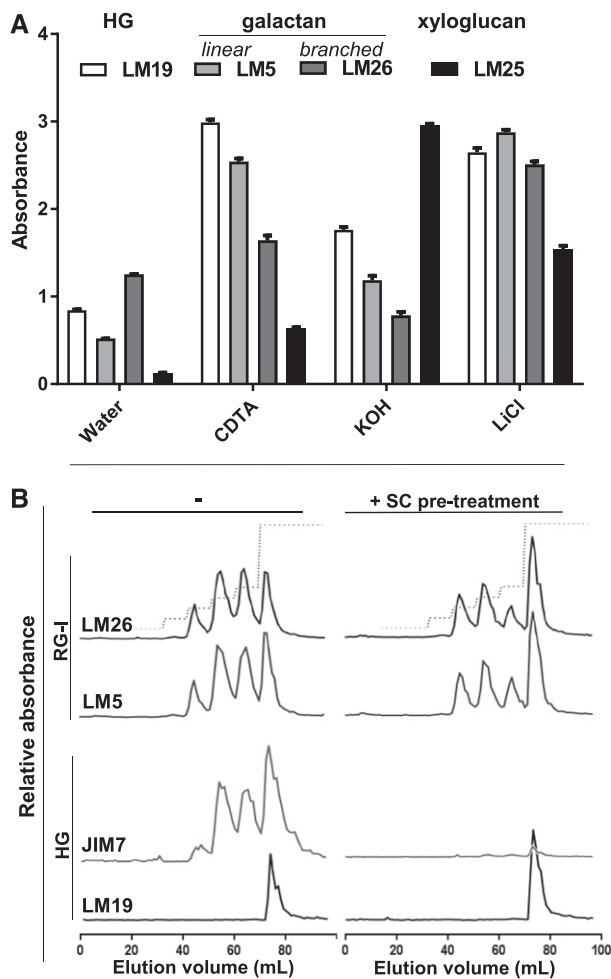
Torode et al.

Figure 4. Analysis of the LM26 epitope solubilized from garlic bulb cell walls. A, ELISA of the LM26 epitope in sequential extractions of increasing stringency of a preparation of garlic bulb cell walls. Comparative data with LM19 HG, LM5 linear galactan, and LM25 xyloglucan epitopes. The LM26 epitope was more abundant in the water-soluble fraction relative to the LM19 and LM5 epitopes. Error bars indicate SD of four technical replicates. Data representative of two biological replicates. B, Epitope detection of anion-exchange chromatography fractions of water-soluble material from garlic bulb AIR using LM26 and LM5 along with pectic HG probes (JIM7, methyl-esterified HG, and LM19 unesterified HG). The stepped salt elution gradient used for the analysis is shown as dashed line on the top chromatographic traces. Traces shown are means of three chromatographic runs. In some cases, samples were pretreated with sodium carbonate to deesterify HG components before chromatographic analyses. The LM26 epitope profile is closely aligned to that of the LM5 epitope and indicates its presence on RG-I molecules, some of which are HG-associated. SC, sodium carbonate.

mechanical features of native cell walls. Unfixed Miscanthus stem material did not survive cryo-sectioning, but the surrounding sheath of leaves survived intact. Analysis of leaf phloem regions further confirmed the complementary patterning of the LM26 and LM5 epitopes, but in this case, there was a declining gradient of LM26 epitope detection from the ventral toward

the dorsal side of leaves (Fig. 7A). This was less pronounced for the LM5 epitope. Analysis of sieve elements and companion cell wall IM across the ventral-dorsal axis of the phloem region also showed a gradient with reduced IM for both cell types toward the dorsal surface (Fig. 7B; representative data of one phloem region). However, sieve elements consistently had a lower IM than neighboring companion cells, supporting the observations made on fixed stem phloem (Fig. 6). Two-way ANOVA of the cell-specific IM across the ventral-dorsal axis of five phloem regions showed there was a large significant difference between cell types ($P = <0.005$) and across the dorsal-ventral axis ($P = <0.05$; Fig. 7C).

In summary, in the phloem tissue of Miscanthus the presence of branched motifs of galactan are concurrent with a lower IM (more elastic cell wall) relative to cell walls in which the linear galactan is predominant.

DISCUSSION

Synthetic Glycan Arrays as a Discovery Platform

Carbohydrate microarrays constitute a powerful technology for the rapid screening of glycan-protein interactions (Fangel et al., 2012; Ruprecht et al., 2017). Microarray slides can be populated with polysaccharides, e.g. AIR extracts from different plant materials, with more defined oligosaccharides from partial degradation/extraction, or with chemically synthesized glycans. Such arrays provide a platform for studying plant cell wall polysaccharides with molecular probes such as MAbs (Pedersen et al., 2012) and for identifying enzymatic activity (Vidal-Melgosa et al., 2015). Well-defined, single-compound oligosaccharides provide the highest resolution possible when characterizing protein-carbohydrate interactions, provided that the binding interactions are sufficiently strong to be detected. This is especially true when a range of structurally related but distinct glycans are available (for examples, see Clausen et al., 2003; Andersen et al., 2016a, 2016b; Schmidt et al., 2015). In the case of LM26 discussed here, it would have been close to impossible to identify the epitope without access to the appropriate and defined linear and branched galactans.

Plant Cell Identity and Cell Surface Molecules

The work of Berger et al. (1994) indicated that stimuli to guide cell identity can reside in cell walls—although the cell wall molecules responsible, in this case from *Fucus*, are not known. There are two major strands of observations that have revealed patterns of cell wall molecules reflecting plant cell types. The first of these is the cell type-specific functional differentiation of cell walls requiring particular glycan components or configurations of cell wall glycans. This is exemplified by the thickened secondary cell walls of xylem vessel elements containing abundant heteroxylan which, in
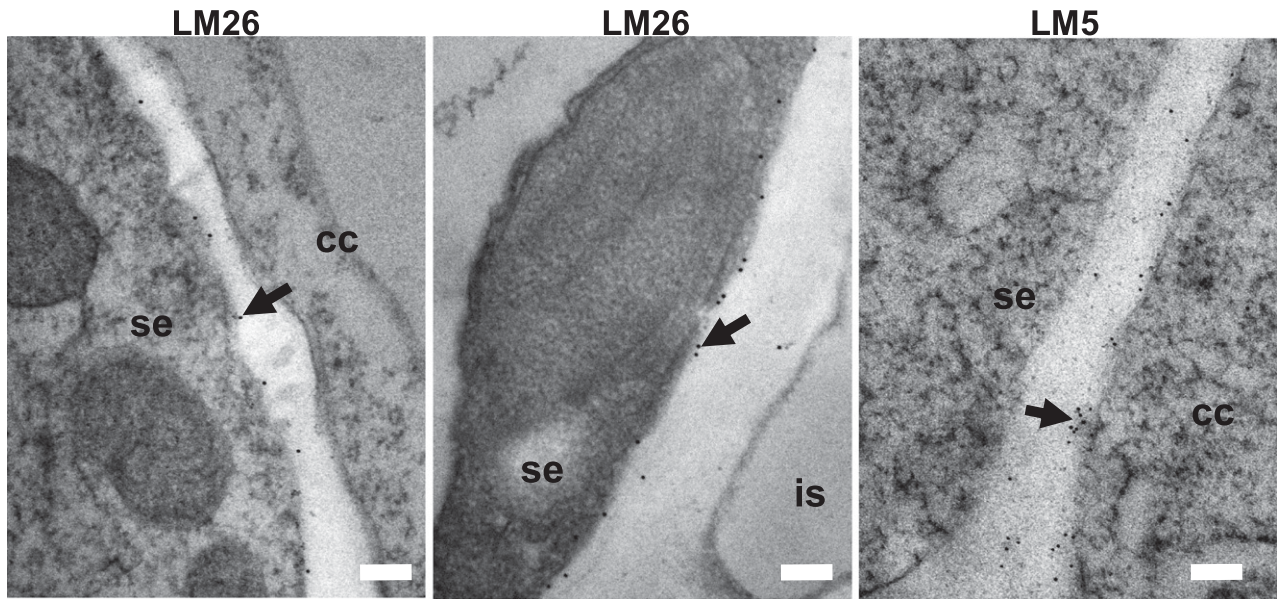
Figure 5. Transmission electron microscopy and immunogold labeling of MAbs LM26 and LM5 binding to phloem regions of transverse sections of Miscanthus stem. Gold particles are restricted to the inner cell-wall regions (marked with arrows) of phloem sieve elements for LM26, and companion cells for LM5. Bars = 200 nm. cc, companion cells; is, intercellular space; se, sieve elements.

eudicots, is present at low levels or absent in primary cell walls of adjacent cells. MAbs directed to heteroxylan are therefore excellent markers of xylem vessel elements in anatomical sections in these systems (McCartney et al., 2005). AGPs and related Hyp-rich glycoproteins display considerable heterogeneity in glycan structures, and glycan epitopes have been related to vascular cell identity in developing organs (Casero et al., 1998; Knox et al., 1989; Smallwood et al., 1994). Indeed, the JIM13 AGP epitope is phloem-specific in maize and onion (*Allium cepa* L.) roots (Casero et al., 1998; Knox 2006), but epitopes such as this appear to be a marker of cell divergence and specification events and not phloem function per se, as the same glycan epitope is a marker of xylem in developing roots of Arabidopsis and other eudicot species (Dolan et al., 1995; Casero et al., 1998). There are clear taxonomic variations in the cell type associations in these classes of glycoprotein epitopes (Casero et al., 1998), and the roles of AGPs/extensins in specifying cell types, if any, are not clear.

The LM26 MAb directed to branched galactan can now contribute to a toolkit of cell wall markers that will facilitate the study of vascular development across a range of angiosperms. The studies could range from analysis of individual cell lineages, to qualitative or quantitative measures of cell wall dynamics during development or cell variation across genetic populations. In the case of sugar beet, the LM26 MAb has the capacity to indicate the phloem cells within the complex system of supernumerary or successive cambia development, and also the potential to link that development with Suc yield in a commercial crop. The significance

of the varying patterns of the detection of the LM26 epitope between systems ranging from restriction to phloem sieve element cell walls to its detection in all cell walls in a tissue as seen for the garlic bulb (Supplemental Fig. S1) is not clear at this stage, but further demonstrates the heterogeneity of plant cell walls.

Functional Role of the Modulation of 1,4-Galactan RG-I Structure in Plant Cell Walls

It is of considerable interest that a branching motif of 1,4-galactan, a component of RG-I, has been identified in sieve elements. The role of RG-I glycans in cell walls is far from clear, but much evidence has accumulated relating these hypervariable domains of the pectic polysaccharides with generation of cell wall mechanical properties. 1,4-Galactan-rich domains can be associated with increased firmness of cell walls (McCartney et al., 2000), are not detected where extensive elastic properties may be required (Lee et al., 2012), and are often degraded during fruit softening processes (Brummell 2005). However, the micromechanical basis of galactan-rich RG-I contributions to cell wall firmness are not known. It has recently been determined that the LM5 epitope encompasses terminal galactosyl residues at the nonreducing end of 1,4-galactan (Andersen et al., 2016b) and this epitope has been specifically located at inner cell wall regions adjacent to plasma membranes (McCartney et al., 2000; Lee et al., 2013)—a location observed for the LM26 branched galactan epitope (Figs. 2 and 5).
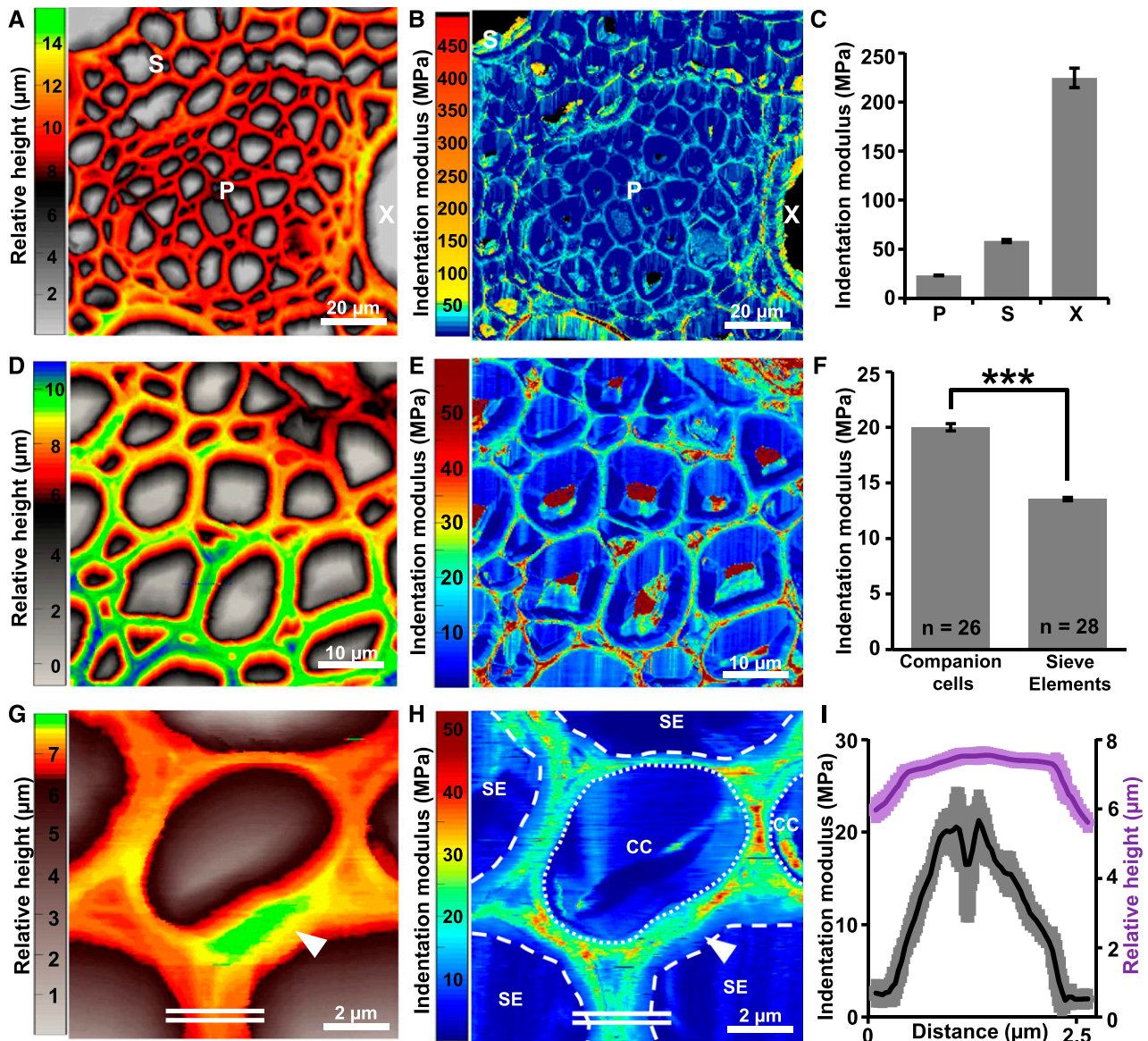
Figure 6. AFM analysis of fixed Miscanthus stem sections. Rows represent analysis at the tissue (A to C), cell (D to F), and submuro (G to I) levels. The left-hand column (A, D, and G) gives set-point height maps of the sections, the middle column (B, E, and H) gives corresponding maps of indentation modulus, and the right column (C, F, and I) shows quantitative data extracted from multiple AFM experiments. C, Indentation moduli of specific cell types. F, Indentation moduli of companion cell and sieve element cell walls. ***, P value of > 0.001 for Wilcoxon statistical analysis. I, Transect across two adjacent sieve element cell walls (equivalent to double white lines in G and H) showing height (purple) and IM (gray). Arrowheads indicate inner cell-wall regions of phloem sieve element cell walls with lower indentation moduli. Scale bars as shown. Error bars = ±se. p, phloem; s, sclerenchyma; x, xylem.

The substitution identified here (branching, possibly at nonreducing termini) may contribute to the modification of 1,4-galactan to enhance the elastic properties required for cell walls under pressure (van Bel 2003). It is of interest that the branched 1,4-galactan epitope in grass sieve element cell walls is associated with the lack of detection of the linear LM5 1,4-galactan epitope that is only readily detected in cell walls of the closely associated companion cells. This suggests that cell-specific modification of the termini of galactosyl side chains of RG-I in response to mechanical requirements or elevated turgor pressures may be a key factor in the hypervariability of RG-I glycans in cell walls. The micromechanical testing of Miscanthus phloem tissues by AFM support this hypothesis in that it indicates the sieve element cell walls are more elastic than companion cell walls and also that it is the inner cell wall regions that are most elastic (Fig. 6). Structural
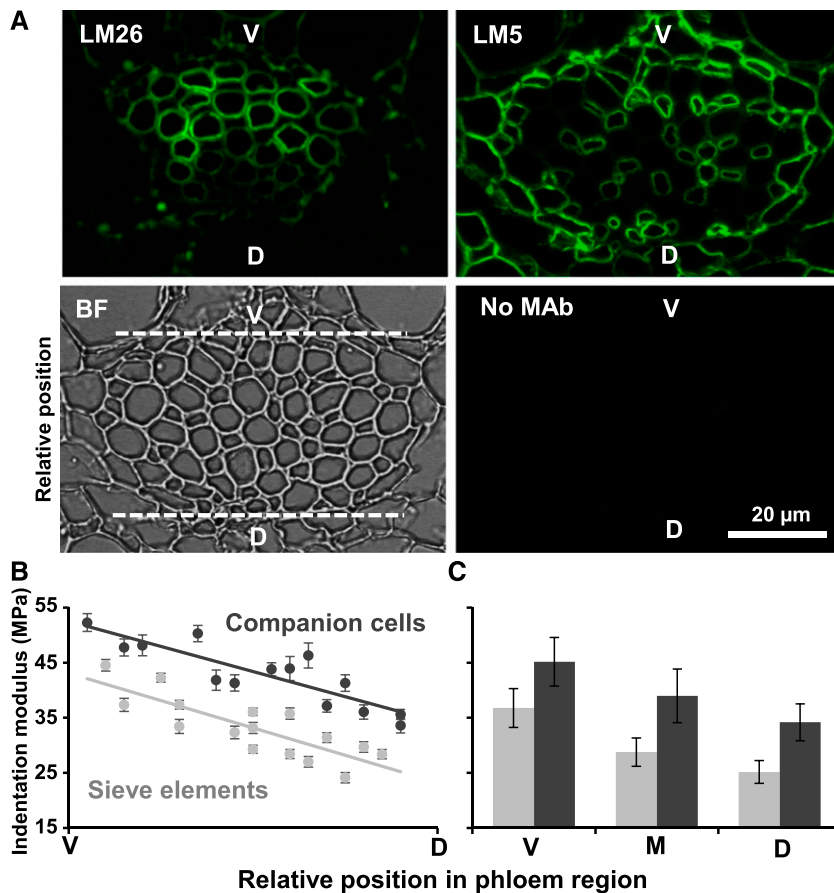
Figure 7. Immunofluorescence and AFM analysis of unfixed, cryo-sectioned Miscanthus leaf phloem. A, Indirect immunofluorescence analysis of MAbs LM26 and LM5 binding to equivalent transverse sections of phloem regions with orientation of ventral and dorsal leaf surfaces. Equivalent bright field and no primary MAb control micrographs are also shown. Horizontal dashed white lines in the bright field micrograph enclose the region analyzed by AFM. Bar = 20 μm. B, AFM analysis of indentation moduli across phloem regions scanned from ventral to dorsal as shown in (A). Representative data from a scan across an individual phloem region are shown and indicate IM data for sieve element and companion cell walls. For each set of assessments, sieve element walls (light gray) had lower IM than associated companion cell walls (dark gray). C, Histogram shows AFM IM data from five phloem regions (separated into ventral, middle, and dorsal regions). Two-way ANOVA analysis revealed that IM is significantly different between cell types (*P* = <0.005) and across the ventral-dorsal axis (*P* = <0.05). Error bars = ±sᴇ. BF, bright field; D, dorsal; M, middle; V, ventral.

modifications to RG-I side chains are likely to influence their capacity to cross link to other cell wall components (Zykwinska et al., 2007), and in this instance to modulate the mechanical forces across the phloem tissue required for optimum phloem tissue function. Interestingly, primary cell walls with elevated tensile mechanical properties such as phloem fibers and tension wood are reported to contain highly branched galactan side chains of RG-I in tight association with cellulose (Roach et al., 2011; Gorshkova et al., 2015). This is in agreement with our observations.

Specific Modulation of Galactan with Regard to Phloem Function

The discovery of a cell wall glycan epitope specific to sieve elements in a range of systems is intriguing. The proposed mass flow of nutrients and photosynthate through phloem sieve elements requires the generation of considerable turgor pressure that is presumably greater than that of surrounding cells (De Schepper et al., 2013; Heo et al., 2014; Knoblauch and Oparka 2012; van Bel 2003). Phloem sieve element cell walls are often thickened compared to adjacent cells but not

to the extent of secondary cell walls of xylem vessel elements. The phloem cells of grass species are not interspersed with parenchyma cells as in most eudicot phloem tissues and the complementary galactan epitope patterning may reflect a need to maintain elastic properties in a tissue with a high density of sieve elements. We propose that the galactan branching motif is a modulation that enhances cell wall elasticity relative to linear galactan. The gradients of both galactan detection and IM values detected across leaf phloem regions may reflect an increase in IM across the phloem tissue during maturation (Fig. 7). This is further suggestive of a link between cell-based modulations of pectic galactan to ensure appropriate mechanical properties for phloem content flow as discussed above. Other aspects of cell wall glycan heterogeneity, influencing both cell wall mechanical properties and/or the detection of epitopes in in situ analyses, may also be relevant in this context.

A hypothesis for function of the radial heterogeneity of cell wall mechanical properties within sieve elements (Fig. 6) is that the more elastic inner cell wall might facilitate the optimization of cytoplasmic diameter via dilation/contraction of the cell wall in response to altered turgor pressure. The radial distribution of elastic

properties may buffer immediate changes in turgor such as diurnal rhythms of phloem and xylem pressure resulting in reversible swelling of sieve tube cell walls (Pfautsch et al., 2015; Knoblauch et al., 2016).

In Muro Testing of Cell Wall Nanomechanics of Nondermal Cells

AFM-based techniques in plant biology have allowed the direct testing of cell wall mechanics on a submuro, cellular, and tissue level (Cosgrove 2016; Bidhendi and Geitmann 2016; Carter et al., 2017). Technically, to-date, analyses of developing plant systems have been limited to readily accessible unadhered cells and surface cell walls of epidermal tissues, with internal tissue mechanics only being inferred by large-scale indentations through multiple cell layers (Peaucelle et al., 2011). Analysis of sectioned plant materials such as wood is carried out routinely (Gindl and Schöberl 2004; de Borst et al., 2012; Farahi et al., 2017). Here we highlight the potential to investigate internal primary cell wall mechanics via use of sectioned plant materials—both fixed/embedded and unfixed/cryo-sectioned—and moreover, the mechanics of adhered cell walls of divergent cell types. This approach allows combined biochemical (here via use of MAbs) and biomechanical analysis of cell walls in nondermal tissues.

MATERIALS AND METHODS

Monoclonal Antibodies

The LM26 rat hybridoma cell line was isolated from a screen of cell lines derived subsequent to immunizations that led to the isolation of the pectic homogalacturonan MAb LM7 (Willats et al., 2001b). It was cloned by standard limiting dilution procedures as described (Willats et al., 2001b). The isotype of LM26 is rat IgG1. LM26 was used in the form of unpurified hybridoma cell culture supernatant for all analyses except for immunogold TEM. Other MAbs used in this study include LM5 to pectic 1,4-galactan (Jones et al., 1997; Andersen et al., 2016b) and JIM7 (Clausen et al., 2003) and LM19 (Verhertbruggen et al., 2009) to pectic homogalacturonan; and xyloglucan MAb LM25 (Pedersen et al., 2012).

Preparation of Plant Materials for Indirect Immunocytochemistry and AFM

Plant materials were collected locally and prepared for anatomical investigation using wax-embedding (McCartney et al., 2005; Xue et al., 2013) or resin-embedding (Lee et al., 2012) procedures. Cryosectioned samples of Miscanthus leaves (from around the second internode) were prepared via embedding tissue in optimal cutting temperature compound (OCT compound; VWR), and processed into 10 μm sections using a cryostat-microtome (Leica Microsystems), and stored at −80°C until use. For light microscopy, sugar beet plants were collected at the eight-leaf stage (20°C, 16 h light: 8 h dark), and samples were taken from 20 mm below the widest diameter of the storage root. Indirect fluorescence immunolabeling procedures were carried out as described (Lee et al., 2012; Xue et al., 2013).

For electron microscopy, sugar beet plants were grown to the four-leaf stage (3 weeks after emergence) in a glasshouse (22°C with natural lighting). The storage root region was sampled from 5 mm below the junction of the hypocotyl and the shoot base. Miscanthus stem samples were taken from the center of the second internode (Xue et al., 2013). All samples were fixed by high pressure freezing using a Leica Microsystems EM HPM100 and stored in liquid nitrogen before freeze substitution using dry ethanol in a Leica Microsystems EM AFS.

After freeze substitution, samples were stored at −20°C for 24 h, then 4°C until resin infiltration. Samples were infiltrated with a dry ethanol/LR White resin series and polymerized under nitrogen at 60°C (for sugar beet) or infiltrated with a dry ethanol/Spurr resin and polymerized at 60°C (Miscanthus, which also had a prefreeze substitution osmium tetroxide treatment). MAb hybridoma supernatants were used neat or concentrated 10-fold by freeze-drying, enriched for immunoglobulin using the Melon Gel IgG Spin purification kit (Thermo Fisher Scientific) followed by concentration (to approximately 12-fold original), and buffer exchange into P-buffered-saline (PBS) using the Vivaspin 2 concentrator (GE Healthcare) as per the manufacturer instructions. A series of 70-nm ultrathin sections were cut using a Leica Microsystems UC7 ultramicrotome and collected on nickel grids coated with Formvar and carbon. After blocking [30 min with 1% (w/v) BSA in PBS-Tween (BSA-PBS)] grids were incubated with the purified LM26 for 1 h at 37°C and then washed (3 × 5 min) with PBS-Tween then blocked again for 30 min before incubation for 1 h at 37°C with the secondary antibody (goat-antirat IgG conjugated to 10 nm gold particles) diluted 1:10 in BSA-PBS. Sections were washed three times with PBS-Tween and twice with dH_2O for 5 min per wash before staining. Sections were poststained with uranyl acetate (15 min) and lead citrate (2 min). Micrographs were obtained using a JEOL 2011 transmission electron microscope at 200 kV and a Gatan Ultrascan CCD camera. Several sections from three individual plants were assessed for gold labeling.

Synthetic Glycan/Galactan Microarrays

The chemical synthesis of glycans 1 to 12 (Fig. 3) has been described previously (Pedersen et al., 2012; Andersen et al., 2016a). Carbohydrate microarray screening was performed as described previously (Andersen et al., 2016a, 2016b). Briefly, deprotected oligosaccharides were functionalized with a heterobifunctional linker 2-(N-methylaminooxy)-1-ethanamine, purified from the excess linker and printed onto NHS-activated Slide-H microarrays from Schott using the ArrayJet Sprint microarray printer. After blocking the microarrays with 50 mM ethanolamine in a 50-mM sodium P buffer pH 9.2, the slides were stained with the antibodies LM5 or LM26 at a 1:100 dilution of hybridoma supernatants in PBS for 2 h. The binding of rat MAbs was detected by Alexa-Fluor 488 goat anti-rat IgG antibody from Thermo Fisher Scientific at a 1:500 dilution in PBS for 2 h. The microarrays were scanned using a GenePix 4400A microarray scanner and the images were quantified using Array-Pro Analyzer 6.3 from Media Cybernetics.

Extraction of Cell Wall Glycans from Garlic Bulbs and Analysis by ELISA and Epitope Detection Chromatography

Garlic (*Allium sativum*) bulb cell walls (25 g) were prepared by chopping a garlic bulb into small pieces that were then frozen and freeze-dried. This material was then blended, and converted into an AIR (Torode et al., 2015) via successive washes with 80%, 90%, and 100% (v/v) ethanol, acetone, and finally methanol/chloroform (2:3 v/v) and left to dry overnight. AIR (2 g) was extracted sequentially with deionized water, 50 mM 1,2-cyclohexanediamine tetraacetic acid (CDTA), and 4 M KOH. Residue remaining after the KOH extract was further extracted to solubilize polysaccharides more tightly associated with cellulose (Gurjanov et al., 2008) as follows: the residue was rinsed in deionized water, acetone, air-dried, and dissolved in 8% (w/v) LiCl in N,N-dimethylacetamide, then precipitated by dropwise addition to water, centrifuged (5 min, 3220 rcf), and the pellet resuspended in water, dialyzed (14-KDa cutoff) and freeze-dried. Water, CDTA, and KOH supernatants were similarly dialyzed (KOH extracts being neutralized with glacial acetic acid first) and freeze-dried. All fractions were used at 50 μg/mL to coat microtiter plates and ELISAs were performed as described (Cornuault et al., 2014). EDC analyses followed the procedures as described (Cornuault et al., 2014). To prepare a water extract for EDC, freeze-dried garlic bulb material was ground to a powder using a TissueLyser (Qiagen; http://www.qiagen.com) for 10 min at 50 oscillations s^{-1} and the powder stored at −20°C until use. The powder (15 mg) was used to produce AIR, which was air-dried overnight. AIR (8 mg) was placed into Eppendorf tubes with two ball bearings and ground using the TissueLyser for 2 min at 50 oscillations s^{-1} followed by 2 mL of water in the TissueLyser for 20 min at the same speed. 12 μL aliquots of this water extract (diluted in 2.5 mL of 20 mM sodium acetate buffer, pH 4.5) was injected into an anion-exchange column (1 mL Hi-Trap ANX FF; GE Healthcare) using a Bio-Rad BioLogic LP system. A step elution gradient was used as follows: 20 mM sodium acetate buffer, pH 4.5 at a flow rate of 1 mL/min from 0 min to 20 min with a step change to 20% 0.6 M NaCl at 20 min, followed by step increases of

0.6 M NaCl at 30 min to 20%, 40 min to 30%, 50 min to 40%, and 60 min to 100%. Ninety-six 1-mL fractions were collected. The collected fractions were adjusted to pH 7 by adding 50 μL of 1 M Na$_2$CO$_3$ before 100 μL of each fraction were incubated overnight at 4°C in microtiter plates for detection with MAbs using ELISA. In some cases, the aliquots of water extract were mixed with an equal volume of 0.1 M sodium carbonate and left at room temperature for 3 h before analysis.

Atomic Force Microscopy Analysis of Miscanthus Stems and Leaves

Transverse sections of Miscanthus organs (fixed and wax-sectioned stems or unfixed and cryo-sectioned leaves) were prepared as above. Sections were probed in a hydrated state (deionized water) on glass slides using a 10-nm diameter paraboloid tip attached to a cantilever (PPP-NCL; Windsor Scientific). The cantilever stiffness was calibrated using thermal resonance as 55.32 N/m. Experiments were performed on a Nano Wizard 3 AFM (JPK Instruments), running JPK control software (version 5.0.73). Experimental data were acquired from five phloem regions of different sections, with a minimum of five companion and sieve element cells analyzed per region. Due to the inconsistent topographical height of sections, artifacts were generated in some instances in the cell lumen likely due to contact geometry deviating from the assumed parabolic shape. To limit our analysis to the cell wall regions alone, data were first plotted and selected based upon the height, which distinguished cell wall material and noncell wall material (Fig. 6). Furthermore, residual root-mean-square error was used to filter aberrant elastic moduli curves. Indentation moduli (after Cosgrove, 2016) were calculated using JPK Data Processing (version 5.0.69; JPK Instruments). Force-indentation curves were produced by background subtraction, set-point height, contact point, and, tip-sample separation calculations. A Hertz-Sneddon model was then fit to each approach curve and an indentation modulus [i.e. Apparent Young's Modulus or Young's Modulus (E)] was calculated as described (Braybrook 2015).

Supplemental Data

The following supplemental materials are available.

Supplemental Figure S1. Immunofluorescence analysis of garlic bulb cell walls using galactan-directed monoclonal antibodies.

Supplemental Figure S2. Immunofluorescence analysis of maize stem phloem regions using galactan-directed monoclonal antibodies.

LITERATURE CITED

Andersen MCF, Boos I, Marcus SE, Kračun SK, Rydahl MG, Willats WG, Knox JP, Clausen MH (2016b) Characterization of the LM5 pectic galactan epitope with synthetic analogues of β-1,4-d-galactotetraose. Carbohydr Res **436:** 36–40

Andersen MCF, Kračun SK, Rydahl MG, Willats WGT, Clausen MH (2016a) Synthesis of β-1,4-linked galactan side chains of rhamnogalacturonan I. Chemistry **22:** 11543–11548

Arifkhodzhaev AO (2000) Galactans and galactan-containing polysaccharides of higher plants. Chem Nat Compound **36:** 229–244

Atmodjo MA, Hao Z, Mohnen D (2013) Evolving views of pectin biosynthesis. Annu Rev Plant Biol **64:** 747–779

Bell CI, Milford GFJ, Leigh RA (1996). Sugar beet. In E. Zamski and A. A. Schaffer, editors, Photoassimilate Distribution in Plants and Crops: Source-Sink Relationships. Marcel Dekker, New York, NY, pp. 691–707

Berger F, Taylor A, Brownlee C (1994) Cell fate determination by the cell wall in early *fucus* development. Science **263:** 1421–1423

Bidhendi AJ, Geitmann A (2016) Relating the mechanics of the primary plant cell wall to morphogenesis. J Exp Bot **67:** 449–461

Braybrook SA (2015) Measuring the elasticity of plant cells with atomic force microscopy. Methods Cell Biol **125:** 237–254

Brummell DA (2005) Cell wall disassembly in ripening fruit. Funct Plant Biol **33:** 103–119

Burton RA, Gidley MJ, Fincher GB (2010) Heterogeneity in the chemistry, structure and function of plant cell walls. Nat Chem Biol **6:** 724–732

Caffall KH, Mohnen D (2009) The structure, function, and biosynthesis of plant cell wall pectic polysaccharides. Carbohydr Res **344:** 1879–1900

Carter R, Woolfenden H, Baillie A, Amsbury S, Carroll S, Healicon E, Sovatzoglou S, Braybrook S, Gray JE, Hobbs J, Morris RJ, Fleming AJ (2017) Stomatal opening involves polar, not radial, stiffening of guard cells. Curr Biol **27:** 2974–2983.e2

Casero PJ, Casimiro I, Knox JP (1998) Occurrence of cell surface arabinogalactan-protein and extensin epitopes in relation to pericycle and vascular tissue development in the root apex of four species. Planta **204:** 252–259

Christ AF, Franze K, Gautier H, Moshayedi P, Fawcett J, Franklin RJM, Karadottir RT, Guck J (2010) Mechanical difference between white and gray matter in the rat cerebellum measured by scanning force microscopy. J Biomech **43:** 2986–2992

Clausen MH, Willats WGT, Knox JP (2003) Synthetic methyl hexagalacturonate hapten inhibitors of anti-homogalacturonan monoclonal antibodies LM7, JIM5 and JIM7. Carbohydr Res **338:** 1797–1800

Cornuault V, Manfield IW, Ralet MC, Knox JP (2014) Epitope detection chromatography: a method to dissect the structural heterogeneity and inter-connections of plant cell-wall matrix glycans. Plant J **78:** 715–722

Cosgrove DJ (2016) Plant cell wall extensibility: connecting plant cell growth with cell wall structure, mechanics, and the action of wall-modifying enzymes. J Exp Bot **67:** 463–476

Das NN, Das A (1977) Structure of the D-galactan isolated from garlic (*Allium sativum*) bulbs. Carbohydr Res **56:** 337–349

de Borst K, Bader TK, Wikete C (2012) Microstructure-stiffness relationships of ten European and tropical hardwood species. J Struct Biol **177:** 532–542

De Schepper V, De Swaef T, Bauweraerts I, Steppe K (2013) Phloem transport: a review of mechanisms and controls. J Exp Bot **64:** 4839–4850

Doblin MS, Pettolino F, Bacic A (2010) Plant cell walls: the skeleton of the plant world. Funct Plant Biol **37:** 357–381

Dolan L, Linstead P, Roberts K (1995) An AGP epitope distinguishes a central metaxylem initial from other vascular initials in the *Arabidopsis* root. Protoplasma **189:** 149–155

Evert RF (2006) Esau's Plant Anatomy, Third Ed. John Wiley, Hoboken, NJ

Fangel JU, Pedersen HL, Vidal-Melgosa S, Ahl LI, Salmean AA, Egelund J, Rydahl MG, Clausen MH, Willats WG (2012) Carbohydrate microarrays in plant science. Methods Mol Biol **918:** 351–362

Farahi RH, Charrier AM, Tolbert A, Lereu AL, Ragauskas A, Davison BH, Passian A (2017) Plasticity, elasticity, and adhesion energy of plant cell walls: nanometrology of lignin loss using atomic force microscopy. Sci Rep **7:** 152

Gindl W, Schöberl T (2004) The significance of the elastic modulus of wood cell walls obtained from nanoindentation measurements. Compos A Appl Sci Manuf **35:** 1345–1349

Gorshkova T, Mokshina N, Chernova T, Ibragimova N, Salnikov V, Mikshina P, Tryfona T, Banasiak A, Immerzeel P, Dupree P, Mellerowicz EJ (2015) Aspen tension wood fibers contain β-(1→4)-galactans and acidic arabinogalactans retained by cellulose microfibrils in gelatinous walls. Plant Physiol **169:** 2048–2063

Gurjanov OP, Ibragimova NN, Gnezdilov OI, Gorshkova TA (2008) Polysaccharides, tightly bound to cellulose in cell wall of flax bast fibre: isolation and identification. Carbohydr Polym **72:** 719–729

Heo J-O, Roszak P, Furuta KM, Helariutta Y (2014) Phloem development: current knowledge and future perspectives. Am J Bot **101:** 1393–1402

Jones L, Seymour GB, Knox JP (1997) Localization of pectic galactan in tomato cell walls using a monoclonal antibody specific to (1→4)-b-D-galactan. Plant Physiol **113:** 1405–1412

Knoblauch M, Oparka K (2012) The structure of the phloem—still more questions than answers. Plant J **70:** 147–156

Knoblauch J, Tepler Drobnitch S, Peters WS, Knoblauch M (2016) In situ microscopy reveals reversible cell wall swelling in kelp sieve tubes: one mechanism for turgor generation and flow control? Plant Cell Environ **39:** 1727–1736

Knox JP (2006) Arabinogalactan-proteins and plant cell development. Foods Food Ingred J Jpn 211: 26–31

Knox JP (2008) Revealing the structural and functional diversity of plant cell walls. Curr Opin Plant Biol 11: 308–313

Knox JP, Day S, Roberts K (1989) A set of cell surface glycoproteins forms a marker of cell position, but not cell type, in the root apical meristem of *Daucus carota* L. Development 106: 47–56

Lee KJD, Cornuault V, Manfield I, Ralet M-C, Knox JP (2013) Multiscale spatial heterogeneity of pectic rhamnogalacturonan-I (RG-I) structural features in tobacco seed endosperm cell walls. Plant J 75: 1018–1027

Lee KJD, Dekkers BJW, Steinbrecher T, Walsh CT, Bacic A, Bentsink L, Leubner-Metzger G, Knox JP (2012) Distinct cell wall architectures in seed endosperms in representatives of the Brassicaceae and Solanaceae. Plant Physiol 160: 1551–1566

McCartney L, Marcus SE, Knox JP (2005) Monoclonal antibodies to plant cell wall xylans and arabinoxylans. J Histochem Cytochem 53: 543–546

McCartney L, Ormerod AP, Gidley MJ, Knox JP (2000) Temporal and spatial regulation of pectic (1→4)-β-D-galactan in cell walls of developing pea cotyledons: implications for mechanical properties. Plant J 22: 105–113

Mullendore DL, Windt CW, Van As H, Knoblauch M (2010) Sieve tube geometry in relation to phloem flow. Plant Cell 22: 579–593

Pattathil S, Avci U, Zhang T, Cardenas CL, Hahn MG (2015) Immunological approaches to biomass characterization and utilization. Front Bioeng Biotechnol 3: 173

Peaucelle A, Braybrook SA, Le Guillou L, Bron E, Kuhlemeier C, Höfte H (2011) Pectin-induced changes in cell wall mechanics underlie organ initiation in Arabidopsis. Curr Biol 21: 1720–1726

Pedersen HL, Fangel JU, McCleary B, Ruzanski C, Rydahl MG, Ralet M-C, Farkas V, von Schantz L, Marcus SE, Andersen MCF, Field R, Ohlin M, et al (2012) Versatile high resolution oligosaccharide microarrays for plant glycobiology and cell wall research. J Biol Chem 287: 39429–39438

Pfautsch S, Renard J, Tjoelker MG, Salih A (2015) Phloem as capacitor: radial transfer of water into xylem of tree stems occurs via symplastic transport in ray parenchyma. Plant Physiol 167: 963–971

Ridley BL, O'Neill MA, Mohnen D (2001) Pectins: structure, biosynthesis, and oligogalacturonide-related signaling. Phytochemistry 57: 929–967

Roach MJ, Mokshina NY, Badhan A, Snegireva AV, Hobson N, Deyholos MK, Gorshkova TA (2011) Development of cellulosic secondary walls in flax fibers requires β-galactosidase. Plant Physiol 156: 1351–1363

Ruprecht C, Bartetzko MP, Senf D, Dallabernadina P, Boos I, Andersen MCF, Kotake T, Knox JP, Hahn MG, Clausen MH, Pfrengle F (2017) A synthetic glycan microarray enables epitope mapping of plant cell wall glycan-directed antibodies. Plant Physiol 175: 1094–1104

Scheller HV, Ulvskov P (2010) Hemicelluloses. Annu Rev Plant Biol 61: 263–289

Schmidt D, Schuhmacher F, Geissner A, Seeberger PH, Pfrengle F (2015) Automated synthesis of arabinoxylan-oligosaccharides enables characterization of antibodies that recognize plant cell wall glycans. Chemistry 21: 5709–5713

Showalter AM (2001) Arabinogalactan-proteins: structure, expression and function. Cell Mol Life Sci 58: 1399–1417

Smallwood M, Beven A, Donovan N, Neill SJ, Peart J, Roberts K, Knox JP (1994) Localization of cell wall proteins in relation to the developmental anatomy of the carrot root apex. Plant J 5: 237–246

Sun JY, Tong J, Zhou J (2006) Application of nano-indenter for investigation of the properties of the elytra cuticle of the dung beetle (*Copris ochus* Motschulsky). IEE Proc Nanobiotechnol 153: 129–133

Torode TA, Marcus SE, Jam M, Tonon T, Blackburn RS, Hervé C, Knox JP (2015) Monoclonal antibodies directed to fucoidan preparations from brown algae. PLoS One 10: e0118366

Torode TA, Siméon A, Marcus SE, Jam M, Le Moigne MA, Duffieux D, Knox JP, Hervé C (2016) Dynamics of cell wall assembly during early embryogenesis in the brown alga *Fucus*. J Exp Bot 67: 6089–6100

Truernit E (2014) Phloem imaging. J Exp Bot 65: 1681–1688

van Bel AJE (2003) The phloem, a miracle of ingenuity. Plant Cell Environ 26: 125–149

Verhertbruggen Y, Marcus SE, Haeger A, Ordaz-Ortiz JJ, Knox JP (2009) An extended set of monoclonal antibodies to pectic homogalacturonan. Carbohydr Res 344: 1858–1862

Vidal-Melgosa S, Pedersen HL, Schückel J, Arnal G, Dumon C, Amby DB, Monrad RN, Westereng B, Willats WGT (2015) A new versatile microarray-based method for high throughput screening of carbohydrate-active enzymes. J Biol Chem 290: 9020–9036

Willats WGT, McCartney L, Mackie W, Knox JP (2001a) Pectin: cell biology and prospects for functional analysis. Plant Mol. Biol. 47: 9–27

Willats WGT, Orfila C, Limberg G, Buchholt HC, van Alebeek G-JWM, Voragen AGJ, Marcus SE, Christensen TMIE, Mikkelsen JD, Murray BS, Knox JP (2001b) Modulation of the degree and pattern of methyl-esterification of pectic homogalacturonan in plant cell walls: implications for pectin methyl esterase action, matrix properties and cell adhesion. J Biol Chem. 276: 19404–19413

Wolf S, Mouille G, Pelloux J (2009) Homogalacturonan methyl-esterification and plant development. Mol Plant 2: 851–860

Wyse R (1979) Parameters controlling sucrose content and yield of sugar beet roots. J Sugar Beet Res 20: 368–385

Xue J, Bosch M, Knox JP (2013) Heterogeneity and glycan masking of cell wall microstructures in the stems of *Miscanthus* x *giganteus*, and its parents *M. sinensis* and *M. sacchariflorus*. PLoS One 8: e82114

Yapo BM (2011) Rhamnogalacturonan-I: a structurally puzzling and functionally versatile polysaccharide from plant cell walls and mucilages. Polym Rev 51: 391–413

Zykwinska A, Gaillard C, Buléon A, Pontoire B, Garnier C, Thibault JF, Ralet MC (2007) Assessment of in vitro binding of isolated pectic domains to cellulose by adsorption isotherms, electron microscopy, and x-ray diffraction methods. Biomacromolecules 8: 223–232